Journal of Mathematical Chemistry Vol. 28, Nos. 1–3, 2000

Potential energy surface exploration with equilibrial paths. Part II: Application

Wolfgang Kliesch *

Max Planck Institute for Mathematics in the Sciences, Leipzig Inselstr. 22–26, D-04109 Leipzig, Germany

Received 28 July 1999

The results of an exploration of an *ab initio* potential energy surface of the C_2H_4O system with equilibrial paths are presented. In particular, four minimizers associated with the product of an elimination reaction and 26 saddle points, among these 14 saddle points of first order, have been located. Furthermore, twelve valley–ridge inflection points and seven double bifurcation points have been detected.

1. Introduction

In the previous paper [1] the equilibrial path concept introduced in [2] has been extended to equilibrial paths that include singular points. The simple singular points are of particular interest because they are associated with the branching of reaction channels on potential energy surfaces (PESs). At a (simple) singular point the symmetry of a nuclear system can be broken. This paper presents the results of an application. An *ab initio* potential energy surface of the C_2H_4O system has been explored with equilibrial paths. In particular, four minimizers associated with the product of an elimination reaction and twenty six saddle points (among these 14 saddle points of first order and nine saddle points of second order) have been located. Furthermore, twelve valley–ridge inflection points and seven double bifurcation points (at which two eigenvalues of the Hessian matrix become zero) have been found. All bifurcation points are non-stationary points. Simple bifurcation points have been observed especially when a group of nuclei begins to rotate in a molecular system. The paths that branch off are connected with the two possible directions of rotation.

All located saddle points of higher than first order are symmetric. All nonsymmetric saddle points are of first order. The second order saddle points connect at least two saddle points of first order (which do not necessarily determine different transition structures). Three second order saddle points have been detected which connect a symmetric and a nonsymmetric saddle point of first order, where even one pair of first order saddle points attains about the same potential energy. These observations indicate

* Present address: University of Applied Sciences Magdeburg-Stendal, Department of Water Management, D-39114 Magdeburg, Germany. E-mail: Wolfgang.Kliesch@wasserwirtschaft.hs-magdeburg.de.

0259-9791/00/1200-0113$18.00/0

that (i) the transition structure of a chemical reaction need not be uniquely determined and (ii) second order saddle points should play some role in advanced reaction theories.

The notations introduced in [1] are kept.

2. Exploration of a C_2H_4O PES

In the present section the results of an exploration of the RHF/6–31G(d) potential energy surface of the C_2H_4O system are reported and discussed. The equilibrial paths have been computed by the procedure EQUIPATH [3] combined with the GAUSSIAN'94 program package [4]. The stationary points $\boldsymbol{p}_{st}$ located by a path tracing have been refined to a maximal force of $2 \cdot 10^{-6}$ H/Bohr and a maximal displacement of $6 \cdot 10^{-6}$ Å by the Berny procedure [5], which is included in GAUSSIAN'94. The figures have been created by means of the program *Gauss View* [6].

Below $\boldsymbol{e}_i$, means the ith eigenvector of a Hessian matrix $\boldsymbol{H}(\boldsymbol{p}_{st})$ whereas $\boldsymbol{v}_i$ means the ith normal mode vector projected on the vectorspace $\mathbb{P}_0$ (the eigenvectors/mode vectors that belong to a zero eigenvalue/frequency are not counted). The order of a stationary point $\boldsymbol{p}_{st}$ is denoted by $\mu(\boldsymbol{p}_{st})$. The angle between the subvector $\dot{\boldsymbol{p}}$ of a tangent vector $\boldsymbol{t} = (\dot{\boldsymbol{p}}, \dot{\rho})^\top$ (cf. [1, section 3.2]) and a reaction vector $\boldsymbol{r}$ is denoted by φ. The matrix $\boldsymbol{S}$ is associated with the C_s-symmetry in the present section. For simplicity the path $\boldsymbol{p}(s)$ of an equilibrial path $z(s) = (\boldsymbol{p}(s), \rho(s))$, which describes the rearrangement of the nuclei, is also called an equilibrial path. Notice that the path $\boldsymbol{p}(s)$ leaves the stationary point in the opposite direction if the reaction vector $-\boldsymbol{r}$ is employed instead of $\boldsymbol{r}$.

Activation path tracings have been started at the acetaldehyde minimizer $\boldsymbol{m}_1$ ($\mathrm{E}(\boldsymbol{m}_1) = -152.9160$ H) and both conformers of vinyl alcohol $\boldsymbol{m}_2$ ($E(\boldsymbol{m}_2) = -152.8889$ H), and $\boldsymbol{m}_3$ ($E(\boldsymbol{m}_3) = -152.8854$ H); see figure 1. The results are summarized in table 1.

Since the initial configurations $\boldsymbol{m}_i$, $i = 1(1)3$, have C_s-symmetry, the Jacobian matrices $\mathbf{h}_2'(z_i)$, $z_i = (\boldsymbol{m}_i, 0)$, have not maximal rank if the reaction vector is antisymmetric; see [1, proposition 6]. Therefore only symmetric normal mode vectors and/or eigenvectors have been employed as activation vectors. For the initial configuration $\boldsymbol{m}_1$ normal mode vectors and eigenvectors have been chosen as a reaction vector to illustrate the influence of the choice of the reaction vector on the outcome. For the vinyl alcohol

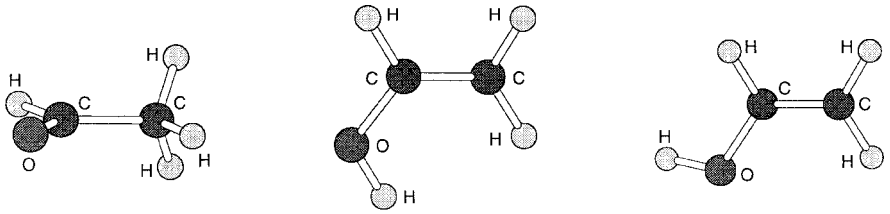

Figure 1. Initial configurations.

Table 1
Results of activation path tracings.

path	$\boldsymbol{p}_0$	$\boldsymbol{r}$	E($\boldsymbol{p}_{tp}$)	$\boldsymbol{p}_b$	E($\boldsymbol{p}_b$)	$\boldsymbol{p}_f$	E($\boldsymbol{p}_f$)	G	μ
1	$\boldsymbol{m}_1$	$\boldsymbol{v}_2$	–	$\boldsymbol{b}_2$	−152.894	–			
2		$-\boldsymbol{v}_2$	−152.779	–		$\boldsymbol{s}_{21}$	−152.7002	C_s	1
3		$\boldsymbol{v}_4$	–	$\boldsymbol{b}_4$	−152.774	–			
4		$-\boldsymbol{v}_4$	–	$\boldsymbol{d}_1$	−152.909	–			
5		$\boldsymbol{v}_5$	−152.777	$\boldsymbol{d}_3$		$\boldsymbol{s}_7$	−152.7646	C_s	2
6		$-\boldsymbol{v}_5$	–	$\boldsymbol{b}_8$	−152.711	–			
7		$\boldsymbol{v}_7$	−152.767	$\boldsymbol{b}_9$	−152.692	$\boldsymbol{s}_{23}$	−152.6811	C_s	3
8		$-\boldsymbol{v}_7$	−152.754	–		$\boldsymbol{s}_{10}$	−152.7392	C_s	2
9		$\boldsymbol{e}_2$	−152.771	–		$\boldsymbol{s}_{26}$	−152.6645	C_s	2
10		$-\boldsymbol{e}_2$	–	$\boldsymbol{d}_2$	−152.914	–			
11		$\boldsymbol{e}_4$	−152.823	–		–			
12		$-\boldsymbol{e}_4$	−152.692	$\boldsymbol{b}_6$	−152.755	$\boldsymbol{s}_7$	−152.7646	C_s	2
13		$\boldsymbol{e}_5$	−152.691	–		–			
14		$-\boldsymbol{e}_5$	−152.771	$\boldsymbol{d}_4$	−152.738	$\boldsymbol{s}_{18}$	−152.7077	C_s	2
15		$\boldsymbol{e}_7$	−152.784	$\boldsymbol{b}_1$	−152.911	$\boldsymbol{s}_{10}$	−152.7392	C_s	2
16		$-\boldsymbol{e}_7$	−152.789	$\boldsymbol{b}_7$	−152.731	–			
17	$\boldsymbol{m}_2$	$\boldsymbol{v}_8$	–	$\boldsymbol{d}_5$	−152.696	$\boldsymbol{s}_{17}$	−152.7213	C_s	3
18	$\boldsymbol{m}_3$	$\boldsymbol{v}_2$	–	$\boldsymbol{b}_3$	−152.868	–			
19		$-\boldsymbol{v}_2$	–	$\boldsymbol{d}_6$	−152.661	$\boldsymbol{s}_{20}$	−152.7021	C_s	2
20		$\boldsymbol{v}_5$	–	$\boldsymbol{b}_4$	−152.811	–			
21		$-\boldsymbol{v}_5$	–	$\boldsymbol{b}_4$	−152.811	–			
22		$\boldsymbol{v}_7$	−152.660	–		$\boldsymbol{s}_{19}$	−152.7057	C_s	1
23		$-\boldsymbol{v}_7$	−152.802	–		$\boldsymbol{s}_3$	−152.8339	C_s	2
24		$\boldsymbol{v}_8$	−152.848	–		$\boldsymbol{s}_3$	−152.8339	C_s	2
25		$-\boldsymbol{v}_8$	−152.708	–		$\boldsymbol{s}_{19}$	−152.7057	C_s	1

Energy in H, G – symmetry group, $\mu = \mu(\boldsymbol{p}_f)$.

minimizers $\boldsymbol{m}_2$ and $\boldsymbol{m}_3$ the inner product $\langle \boldsymbol{m}_i \mid \boldsymbol{r} \rangle$ vanishes such that the initial points of the activation paths 17–26 are singular points by [1, proposition 4]. This drawback has been overcome by fixing the z-coordinate of the carbon nuclei. This trick is justified by [1, theorem 8].

Most activation paths listed in table 1 are not regular equilibrial paths because they include a bifurcation point. The equilibrial paths that include one bifurcation point can be decomposed into two regular equilibrial paths, namely a regular equilibrial path that joins the initial point $(\boldsymbol{p}_0, 0)$ and the bifurcation point $(\boldsymbol{p}_b, \rho_b)$ and a regular equilibrial path that joins the bifurcation point and the final point $(\boldsymbol{p}_f, 0)$.

Along all regular activation paths the C_s-symmetry is conserved in accordance with [1, theorem 8]. Therefore the regular activation paths of finite length end either at a C_s-symmetric saddle point (paths 2, 8, 9 and 22–25) or at a C_s-symmetric bifurcation configuration $\boldsymbol{p}_b$ (paths 1, 3–7, 10, 12, 14–21); cf. [1, theorem 4]. The saddle point configurations (found by following an activation or a relaxation path) are depicted in

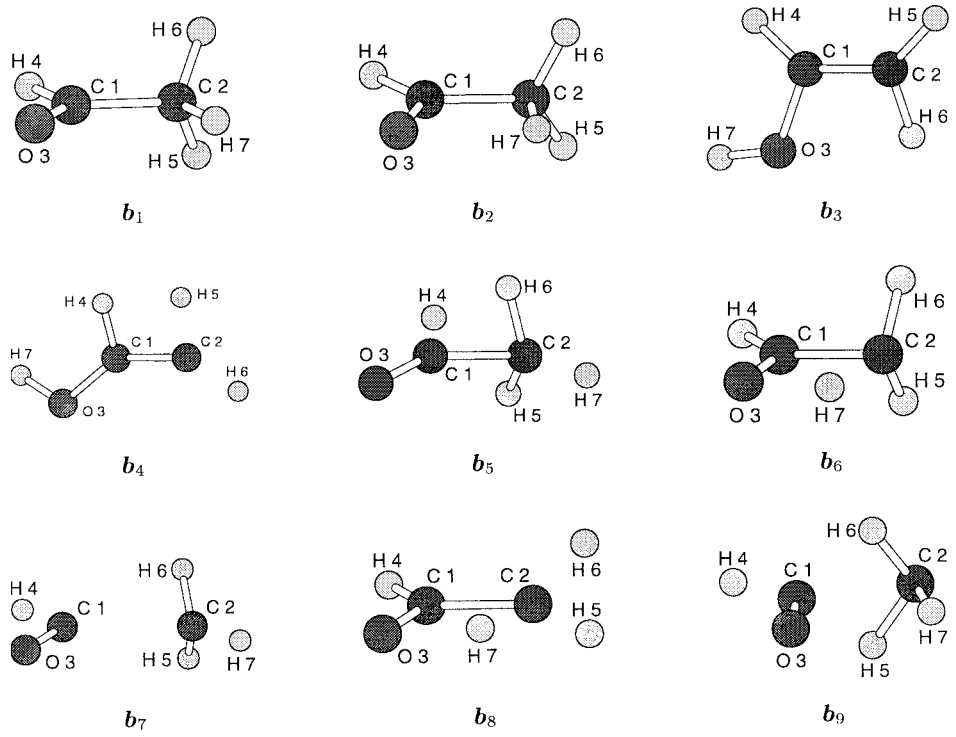

Figure 2. Valley–ridge inflection configurations.

the figures 4–6 (the numbers of the subfigures coincide with the numbers of the saddle points). The internal coordinates are collected in the tables 7–9. The paths 11 and 13 do not return to the hyperplane $\mathbb{P} \times \{0\}$. They run into regions where the potential energy is very high.

Let us consider the regular activation paths of finite length in greater detail now. First the paths that end at a saddle point are to be discussed. These paths pass through one and only one turning point which indicates the entry in the reactive domain. At the turning point one and only one eigenvalue that belongs to a symmetric eigenvector of the Hessian matrix changes its sign; see [1, theorem 10]. Although only one eigenvalue changes its sign, five paths end at a saddle point of second order (paths 8, 9, 23 and 24) and only three paths (2, 22, 25) end at a saddle point of first order. The reason is the following: When an activation path leaves the initial point the zero eigenvalues of the Hessian matrix which belong to the space of infinitesimal rotations become positive or negative. At the final point of the path three eigenvalues become zero. Frequently the number of eigenvalues that become negative in the vicinity of the initial point does not coincide with the number of negative eigenvalues that become zero at the final point; see tables 3 and 4. At all first order saddle points the negative eigenvalue of the Hessian matrix belongs to a symmetric eigenvector. At the second order saddle points the Hessian matrix possesses a symmetric and an antisymmetric eigenvector which belong to a neg-

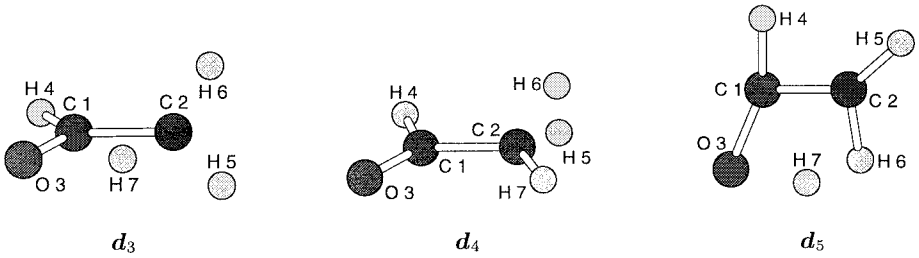

$\boldsymbol{d}_3$ $\boldsymbol{d}_4$ $\boldsymbol{d}_5$

Figure 3. Bifurcation configurations with double zero eigenvalue.

ative eigenvalue. The negative eigenvalues that belong to a symmetric eigenvector result from the change of the sign at the turning point. The negative eigenvalues that belong to an antisymmetric eigenvector are due to a zero eigenvalue of the Hessian matrix $\boldsymbol{H}(\boldsymbol{m}_i)$ which belongs to an antisymmetric vector of infinitesimal rotation and which becomes negative when the path leaves the initial point.

The regular activation paths that end at a bifurcation point end either at a simple bifurcation point $\boldsymbol{\psi}_i = (\boldsymbol{b}_i, \rho_i)$ or at a double bifurcation point $\boldsymbol{\vartheta}_i = (\boldsymbol{d}_i, \rho_i)$. The points $\boldsymbol{\psi}_i$ and $\boldsymbol{\vartheta}_i$ are only approximations to the true bifurcation points. At present the approximations cannot be refined because appropriate codes are not available. The points $\boldsymbol{b}_i$, which are valley–ridge inflection points, are visualized in figure 2. Their internal coordinates are collected in table 10. All points $\boldsymbol{\psi}_i$ excluding the points $\boldsymbol{\psi}_3$ and $\boldsymbol{\psi}_7$ are symmetry-breaking pitchfork bifurcation points; see table 12. At the bifurcation points $\boldsymbol{\psi}_3$ and $\boldsymbol{\psi}_7$ two symmetric branches cross each other. The configurations $\boldsymbol{b}_1$ and $\boldsymbol{b}_2$ are very similar but their kernel vectors are quite different; see table 12. The arclength of the activation path 15 between the initial point and $\boldsymbol{\psi}_1$ is about 0.2 Å, whereas the arclength of the activation path 1 between the initial point and the bifurcation point $\boldsymbol{\psi}_2$ is about 4 Å. The potential energy surface is very flat along path 1 ($\mathrm{E}(\boldsymbol{m}_1) - \mathrm{E}(\boldsymbol{b}_2) =$ 0.6 eV).

The configurations defined by the points $\boldsymbol{d}_3$, $\boldsymbol{d}_4$ and $\boldsymbol{d}_5$ are depicted in figure 3. The configurations $\boldsymbol{d}_1$ and $\boldsymbol{d}_2$ have the appearance of the configurations $\boldsymbol{b}_1$ and $\boldsymbol{b}_2$. The point $\boldsymbol{d}_6$ is only of little importance because the energy is very high at that point. The points $\boldsymbol{\vartheta}_2$, $\boldsymbol{\vartheta}_3$, $\boldsymbol{\vartheta}_5$ and $\boldsymbol{\vartheta}_6$ are symmetry-breaking double turning points. At the points $\boldsymbol{d}_1$ and $\boldsymbol{d}_4$ both zero eigenvalues of the Hessian matrix belong to antisymmetric eigenvectors. In contrast to the points $\boldsymbol{b}_i$ the approximations $\boldsymbol{d}_i$ are poor. Therefore no internal coordinates are given.

The first segment of the activation path 5 ends at the symmetry-breaking double turning point $\boldsymbol{\vartheta}_3$. The primary path, which is symmetric, leads back to a point $\boldsymbol{z}_* = (\boldsymbol{p}_*, \rho_*)$ nearby the initial point $(\boldsymbol{m}_1, 0)$. Thereupon the path runs to the saddle point $\boldsymbol{s}_7$. The point $\boldsymbol{z}_*$ is a turning point (or a bifurcation point?). In the following only the segment of the path that joins the saddle point $\boldsymbol{s}_7$ and the point $\boldsymbol{p}_*$ is considered. The nonsymmetric branches originating at $\boldsymbol{\vartheta}_3$ should lead to the saddle points $\boldsymbol{s}_6$ and $\boldsymbol{S}\boldsymbol{s}_6$. The activation paths 20 and 21 end at bifurcation points that define the same configuration, but they do not end at the same point.

Table 2
Results of relaxation path tracings.

path	$\boldsymbol{p}_0$	G	$\mu(\boldsymbol{p}_0)$	$\boldsymbol{r}$	$\boldsymbol{p}_f$	G	$\mu(\boldsymbol{p}_f)$
1	$\boldsymbol{s}_{25}$	C_s	3	$\boldsymbol{v}_1^s$	$\boldsymbol{s}_9$	C_s	1
2				$\boldsymbol{v}_2^s$	$\boldsymbol{s}_{22}$	C_s	2
3				$\boldsymbol{v}_2^s + \boldsymbol{v}_3^a$	$\boldsymbol{s}_{24}$	C_s	2
4	$\boldsymbol{s}_{23}$	C_s	3	$\boldsymbol{e}_1^s$	—		
5				$\boldsymbol{v}_2^s$	$\boldsymbol{s}_{22}$	C_s	2
6				$\boldsymbol{e}_3^a$	—		
7	$\boldsymbol{s}_{17}$	C_s	3	$\boldsymbol{v}_1^a$	$\boldsymbol{s}_6$	C_1	1
8				$\boldsymbol{v}_2^s$	$\boldsymbol{d}_{15}$	C_s	2
9				$\boldsymbol{e}_3^a$	—		
10	$\boldsymbol{s}_{24}$	C_s	2	$\boldsymbol{e}_1^s$	—		
11				$\boldsymbol{v}_2^a$	$\boldsymbol{s}_9$	C_s	1
12	$\boldsymbol{s}_{22}$	C_s	2	$\boldsymbol{v}_1^s$	$\boldsymbol{s}_{25}$	C_s	3
13				$-\boldsymbol{v}_1^s$	$\boldsymbol{s}_1$	C_s	1
14				$\boldsymbol{e}_1^s$	$\boldsymbol{s}_{23}$	C_s	3
15				$\boldsymbol{e}_2^a$	$\boldsymbol{s}_{12}$	C_1	1
16	$\boldsymbol{s}_{20}$	C_s	2	$-\boldsymbol{e}_1^s$	$\boldsymbol{s}_4$	C_s	1
17				$\boldsymbol{v}_1^s + \boldsymbol{v}_2^a$	$\boldsymbol{s}_{16}$	C_1	1
18	$\boldsymbol{s}_{18}$	C_s	2	$\boldsymbol{e}_1^a$	$\boldsymbol{s}_{13}$	C_1	1
19				$-\boldsymbol{e}_2^s$	$\boldsymbol{s}_8$	C_s	1
20	$\boldsymbol{s}_{15}$	C_s	2	$\boldsymbol{v}_1^a$	$\boldsymbol{s}_{11}$	C_1	1
21				$\boldsymbol{e}_2^a$	—		
22	$\boldsymbol{s}_{10}$	C_s	2	$\boldsymbol{e}_1^s$	—		
23				$\boldsymbol{v}_1^s + \boldsymbol{v}_2^a$	$\boldsymbol{s}_9$	C_1	1
24	$\boldsymbol{s}_7$	C_s	2	$\boldsymbol{e}_1^s$	$\boldsymbol{s}_5$	C_s	1
25				$\boldsymbol{m}_2^a$	$\boldsymbol{s}_6$	C_1	1
26	$\boldsymbol{s}_3$	C_s	2	$\boldsymbol{v}_1^s$	$\boldsymbol{m}_3$	C_s	0
27				$\boldsymbol{v}_1 + \boldsymbol{v}_2^a$	$\boldsymbol{s}_2$	C_1	1
28	$\boldsymbol{s}_{19}$	C_s	1	$\boldsymbol{v}_1^s$	$\boldsymbol{m}_4$	C_s	0
29	$\boldsymbol{s}_{16}$	C_1	1	$-\boldsymbol{e}_1$	$\boldsymbol{m}_6$	C_s	0
30	$\boldsymbol{s}_{14}$	C_1	1	$-\boldsymbol{e}_1$	$\boldsymbol{m}_7$	C_s	0
31	$\boldsymbol{s}_{11}$	C_1	1	$-\boldsymbol{e}_1$	—		
32	$\boldsymbol{s}_{13}$	C_1	1	$-\boldsymbol{e}_1$	—		
33	$\boldsymbol{s}_9$	C_s	1	$\boldsymbol{e}_1^s$	$\boldsymbol{m}_0$	C_s	0
34	$\boldsymbol{s}_8$	C_s	1	$-\boldsymbol{e}_1^s$	—		
35	$\boldsymbol{s}_6$	C_1	1	$\boldsymbol{e}_1$	$\boldsymbol{m}_2$	C_s	0
36	$\boldsymbol{s}_2$	C_1	1	$-\boldsymbol{e}_1$	$\boldsymbol{m}_3$	C_s	0

^{s} symmetric vector, ^{a} antisymmetric vector

If a bifurcation point is encountered the path tracing is continued along the symmetric branch (at present the program EQUIPATH cannot change to a nonsymmetric branch). Thus the paths 5, 7, 12, 14, 15 and 19 end at a symmetric saddle point. Along the activation paths 5 and 15 a turning point was encountered after passing through the bifurcation point.

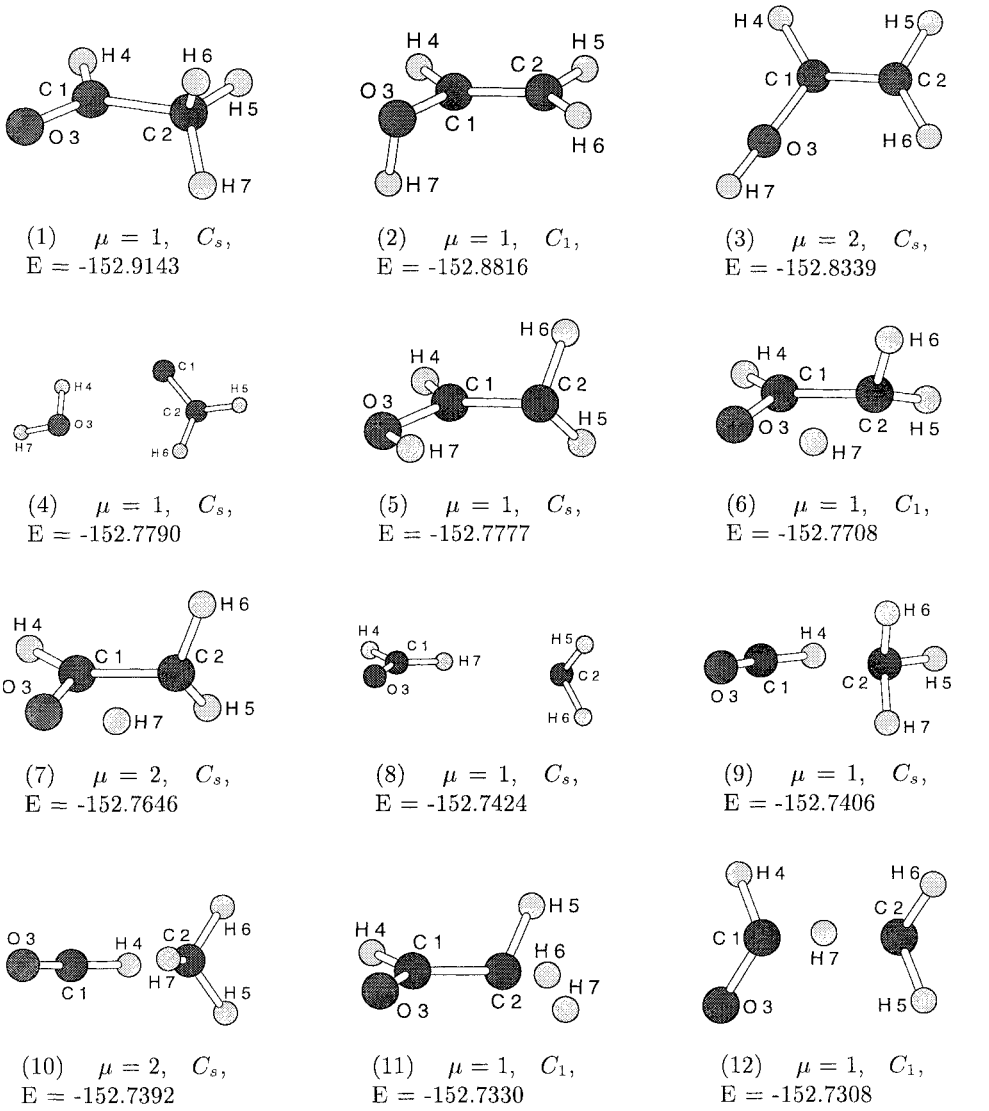

Figure 4. Saddle point configurations.

At the saddle points of higher order and some first order saddle points relaxation path tracings have been started. Table 2 shows the results. The columns of table 2 which are headed by $\boldsymbol{r}$ (reaction vector) and $\boldsymbol{p}_f$ (final point) are to read as follows: If no stationary point has been located using an eigenvector $\boldsymbol{e}_i$ then a stationary point was found neither using the eigenvector $\boldsymbol{e}_i$, nor using the projected normal mode vector $\boldsymbol{v}_i$.

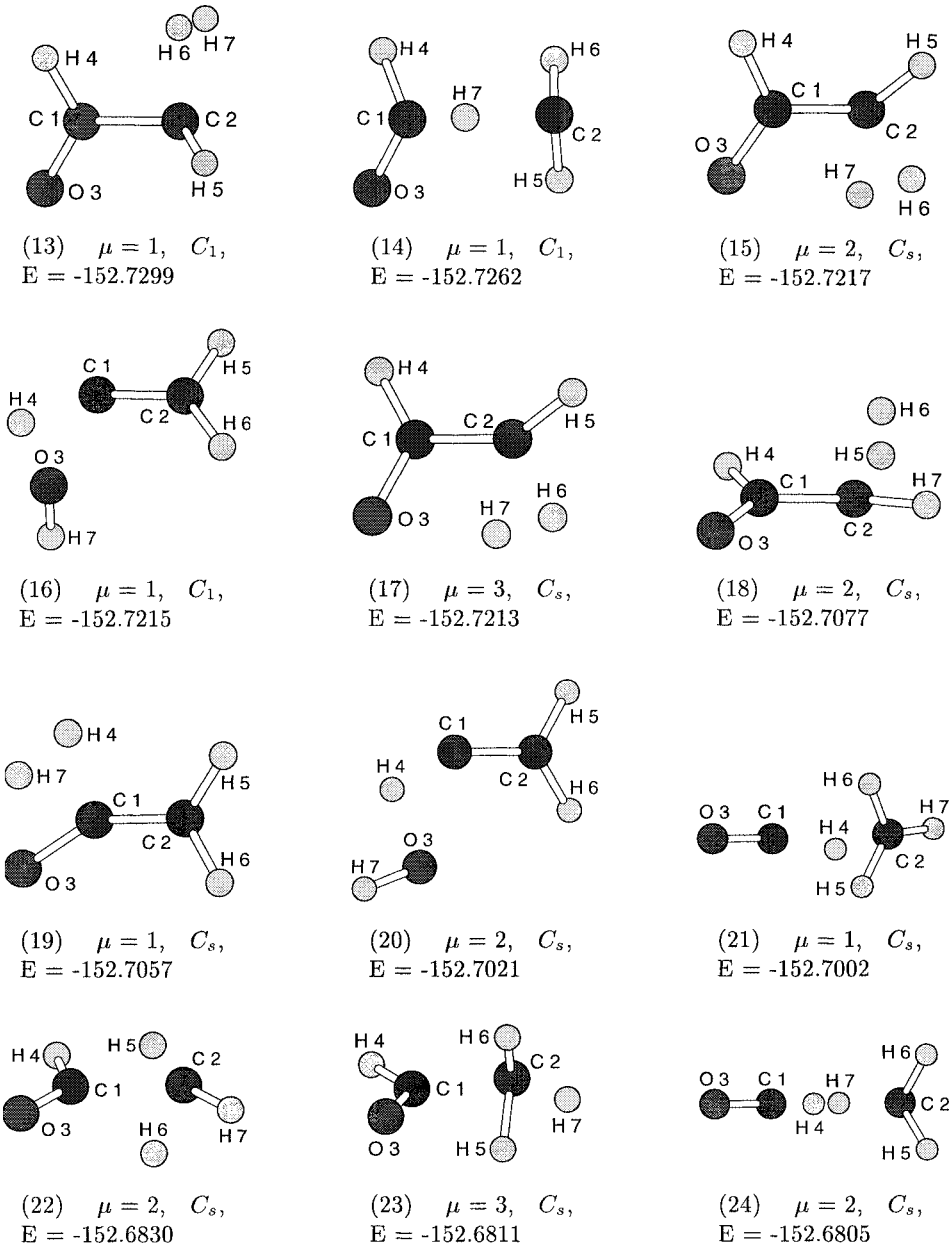

Figure 5. Saddle point configurations.

All saddle points ***s*** of higher than first order have C_s-symmetry. Therefore, if the reaction vector ***r*** is antisymmetric, the initial point is singular, i.e., there is no uniquely determined initial tangent to the relaxation path; cf. [1, proposition 6]. But frequently a first regular point at the antisymmetric branch is obtained if the initial tangent ***t*** is

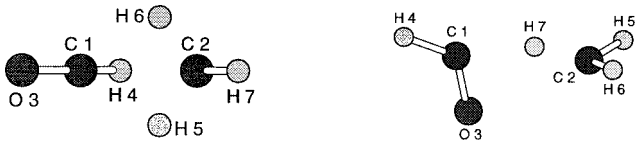

(25) $\mu = 3, \quad C_s,$
E = -152.6736

(26) $\mu = 2, \quad C_s,$
E = -152.6645

Figure 6. Saddle point configurations.

calculated from the equation

$$\left(\boldsymbol{H}(\boldsymbol{s}) + \sum_{i=1}^{3} \boldsymbol{u}_i \boldsymbol{u}_i^{\top} + \sum_{i=1}^{3} (\boldsymbol{u}_i \times \boldsymbol{s})(\boldsymbol{u}_i \times \boldsymbol{s})^{\top} \right) \boldsymbol{t} = \boldsymbol{0}.$$

(Unfortunately this trick does not work for activation paths. A reason may be that the initial tangents to the antisymmetric branches are not perpendicular to the vectors of infinitesimal rotation.)

Let us consider the relaxation paths that originate at a saddle point of higher order in greater detail. The paths determined by a symmetric reaction vector lead to a symmetric stationary point whereas the paths determined by an antisymmetric reaction vector end at an antisymmetric (paths 7, 15, 18, 20, 25) *or* a symmetric stationary point (path 11). Most relaxation paths end at a stationary point $\boldsymbol{p}_f$ of the order $\mu(\boldsymbol{p}_0) - 1$, but a relaxation path need not necessarily end at a stationary point which order is lower than that of the initial point; see relaxation paths 12 and 14. The relaxation paths that start at a first order saddle point end at a minimizer (or fail). Notice that all minimizers have C_s-symmetry. The energies and the internal coordinates of the minimizers which are different from the initial configurations are listed in table 6. Illustrations of the configurations are found in the figures 9–12. The minimizer $\boldsymbol{m}_0$ appears to be the global minimizer of the C_2H_4O potential energy surface (no lower minimum has been found). Several paths pass through a bifurcation point. The important bifurcation points are discussed in conjunction with the reaction topography in the sections.

The final point of path 19 possesses only a very small imaginary frequency ($\nu_1 = -36.5\mathrm{i}\,\mathrm{cm}^{-1}$), but $\boldsymbol{s}_8$ is a saddle point indeed. Along the eigenvector $\boldsymbol{e}_1$ a decrease in the potential energy has been observed. Additionally to the small imaginary frequency the transition structure $\boldsymbol{s}_8$ possesses two very small harmonic frequencies ($\nu_2 = 44.8\ \mathrm{cm}^{-1}$, $\nu_3 = 88.2\ \mathrm{cm}^{-1}$) which belong to antisymmetric normal mode vectors (rotation of $\overline{\mathrm{C}}\mathrm{H}_2$ about its symmetry axis and rotation of formaldehyde about the CO axis, respectively).

Along the paths 31 and 32 the hydrogen molecule moves away from the $\mathrm{H}\overline{\mathrm{C}}\mathrm{CHO}$ fragment.

Path 34 approaches the minimizer $\boldsymbol{m}_7$ first, but then it moves away and breaks down. It appears that the path runs on a plateau.

The first harmonic frequency of the transition structure $\boldsymbol{s}_4$ is very small ($\nu_2 = 54.0\ \mathrm{cm}^{-1}$). It belongs to the (antisymmetric) normal mode vector which is associated

with the rotation of the $H_2C\overline{C}$ fragment about the CC axis. Also the structures $\boldsymbol{s}_{23}$, $\boldsymbol{s}_{24}$ and $\boldsymbol{s}_{25}$ possess a very small harmonic frequency which is smaller than 83 cm^{-1}.

Notice that all saddle points of second or third order are symmetric. All nonsymmetric saddle points are of first order.

In the sections the equilibrial paths are connected with reactions.

2.1. Change of conformation in vinyl alcohol

The change of the conformation in vinyl alcohol is related to the activation path 23 (table 1) and the relaxation paths 26, 27 and 36 (table 2). All configurations of the activation path 23 and the relaxation path 26 are planar in accordance with [1, theorem 8].

The behavior of the small eigenvalues of the Hessian matrix along the activation path 23 ($\boldsymbol{p}_0 = \boldsymbol{m}_3$, $\boldsymbol{p}_f = \boldsymbol{s}_3$) shows table 3 (the zero eigenvalues belonging to the space of overall translations are always left out of account). The first eigenvalue changes its sign between the first and the second point. The eigenvector is antisymmetric and therefore it is perpendicular to the gradient, which is symmetric. Thus the change of the sign indicates a symmetry-breaking bifurcation point; cf. [1, theorem 10]. But the positive sign of the eigenvalue λ_1 at the first point may also be caused by a poor approximation. Therefore we cannot say definitely that there is a simple bifurcation point in the vicinity of the initial point $(\boldsymbol{m}_1, 0)$. Table 3 proves further that point 28 is an approximate turning point ($\dot{\boldsymbol{p}} \approx 0$, $\dot{\boldsymbol{p}} \in \mathbb{P}_s$ and $\varphi = \langle \boldsymbol{r} \mid \dot{\boldsymbol{p}} \rangle \neq 0$; cf. [1, theorem 10]). At the 33rd point the angle φ is about 90°, but no eigenvalue changes its sign in the vicinity of this point. Thus the point is a (local) maximizer along the activation path and the path of the nuclear configurations approaches the saddle point from above.

The relaxation path 26, which originates at the second order saddle point $\boldsymbol{s}_3$, ends at the minimzer $\boldsymbol{m}_3$ although it passes only through one turning point and no bifurcation

Table 3
Characteristic values along the activation path 23.

i	λ_1	λ_2	λ_3	λ_4	λ_5	$\dot{\rho}$	φ
0	0.0000^a	0.0000^s	0.0000^a	0.0026^a	0.0248^s	0.073	—
1	0.0001^a	0.0002^a	0.0002^s	0.0019^a	0.0250^s	0.072	22.8
2	-0.0002^a	0.0003^a	0.0005^s	0.0017^a	0.0251^s	0.072	20.2
⋮	⋮	⋮	⋮	⋮	⋮	⋮	⋮
28	-0.0849^a	$\underline{0.0004}^s$	0.0050^a	0.0082^s	0.0100^a	0.006	60.4
29	-0.0886^a	$\underline{-0.0074}^s$	0.0050^a	0.0078^s	0.0100^a	−0.006	66.8
⋮	⋮	⋮	⋮	⋮	⋮	⋮	⋮
32	-0.0993^a	-0.0331^s	0.0049^a	0.0074^s	0.0099^a	−0.038	85.1
33	-0.1028^a	-0.0420^s	0.0050^a	0.0074^s	0.0099^a	−0.047	90.5
34	-0.1064^a	-0.0512^s	0.0048^a	0.0073^s	0.0097^a	−0.057	96.3
⋮	⋮	⋮	⋮	⋮	⋮	⋮	⋮
76	-0.2227^a	-0.0074^s	0.0000^a	0.0000^s	0.0000^a	−0.070	118.4

^{s} symmetric eigenvector, ^{a} antisymmetric eigenvector, λ_i in mdyn/Å, φ in degrees

Table 4
Eigenvalues of the Hessian matrix along the activation path 17.

i	λ_1	λ_2	λ_3	λ_4	λ_5	λ_6
0	0.0000^a	0.0000^s	0.0000^a	0.0120^a	0.0217^s	0.0509^a
1	-0.0002^a	-0.0001^s	-0.0001^a	0.0124^a	0.0220^s	0.0514^a
⋮	⋮	⋮	⋮	⋮	⋮	⋮
52	-0.0634^a	-0.0148^s	-0.0130^a	0.0001^a	0.0175^s	0.0358^a
53	-0.0638^a	-0.0149^s	-0.0131^a	$\underline{0.0000}^a$	$\underline{0.0079}^s$	0.0358^a
54	-0.0647^a	-0.0150^s	-0.0132^a	$\underline{-0.0047}^s$	$\underline{-0.0001}^a$	0.0354^a
55	-0.0657^a	-0.0157^s	-0.0136^s	-0.0132^a	-0.0006^a	0.0348^a
⋮	⋮	⋮	⋮	⋮	⋮	⋮
102	-0.0561^a	-0.0394^s	-0.0003^a	-0.0002^s	-0.0002^a	0.0016^a
103	-0.0575^a	-0.0339^s	-0.0002^a	-0.0002^s	-0.0001^a	0.0006^a
104	-0.0592^a	-0.0281^s	-0.0005^a	-0.0001^a	-0.0001^s	0.0000^a
105	-0.0605^a	-0.0242^s	-0.0013^a	0.0000^a	0.0000^s	0.0000^a

^{s} symmetric eigenvector, ^{a} antisymmetric eigenvector, λ_i in mdyn/Å.

point. The reason is that two of the three zero eigenvalues which belong to the space of infinitesimal rotations at the saddle point become negative when the path leaves the saddle point whereas in the vicinity of the final point three negative eigenvalues of the Hessian matrix tend to zero. The relaxation path 27, which also originates at $\boldsymbol{s}_3$, passes through a turning point and ends at the first order saddle point $\boldsymbol{s}_2$.

The relaxation path 36 ($\boldsymbol{p}_0 = \boldsymbol{s}_2$) ends in the vicinity of the minimzer $\boldsymbol{m}_3$. Along this path small displacements ($< 10^{-4}$ Å in the Euclidean norm) cause a large increase in the potential energy (1–2 eV). Obviously the relaxation path follows a flat ($\mathrm{E}(\boldsymbol{m}_3) - \mathrm{E}(\boldsymbol{s}_2) = 0.1$ eV) and very small valley of the potential energy surface. It appears that there is a bifurcation point very close to the final point $(\boldsymbol{m}_3, 0)$. The nonsymmetric branches should lead to the saddle points $\boldsymbol{s}_2$ and $\boldsymbol{S}\boldsymbol{s}_2$ whereas the symmetric branch leads to the minimizer $\boldsymbol{m}_3$.

The results indicate that there exist a circular valley that joins the transition structures $\boldsymbol{s}_2$ and $\boldsymbol{S}\boldsymbol{s}_2$ (rotation of H about the CO axis) and two side-valleys which branch off from the circular valley and lead to the conformers $\boldsymbol{m}_2$ and $\boldsymbol{m}_3$. The hypothesis is visualized in figure 7.

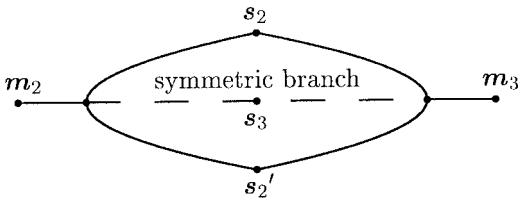

Figure 7. Change of conformation in vinyl alcohol.

Table 5
Characteristic values along the relaxation path 28.

i	λ_1	λ_2	λ_3	λ_4	λ_5	$\dot{\rho}$	φ
0	-0.4642^s	0.0000^a	0.0000^s	0.0000^a	0.0192^a	0.312	—
1	-0.4408^s	-0.0023^a	-0.0002^s	0.0005^a	0.1949^a	0.360	129.5
⋮	⋮	⋮	⋮	⋮	⋮	⋮	⋮
21	-0.1557^s	-0.0272^a	-0.0060^s	0.0002^a	0.0061^a	0.067	102.8
22	-0.1302^s	-0.0286^a	-0.0066^s	$\underline{0.0000}^a$	0.0055^a	0.061	102.8
23	-0.1092^s	-0.0299^a	-0.0071^s	-0.0004^a	0.0051^a	0.057	104.7
⋮	⋮	⋮	⋮	⋮	⋮	⋮	⋮
29	-0.0331^a	-0.0195^s	$\underline{-0.0026}^s$	-0.0018^a	0.0038^a	0.011	113.7
30	-0.0332^a	-0.0156^s	-0.0020^a	$\underline{-0.0014}^s$	0.0037^a	0.001	115.8
31	-0.0331^a	-0.0140^s	-0.0022^a	0.0036^a	0.0043^s	−0.007	117.2
⋮	⋮	⋮	⋮	⋮	⋮	⋮	⋮
87	0.0000^a	0.0000^s	0.0000^a	0.0000^a	0.0001^s	−0.002	129.5

^{s} symmetric eigenvector, ^{a} antisymmetric eigenvector, λ_i in mdyn/Å, φ in degrees

2.2. Tautomerization in vinyl alcohol/acetaldehyde

The intramolecular tautomerization in the vinyl alcohol/acetaldehyde system has been studied by Andrés et al. [7] very recently.

First an equilibrial path tracing has been started at the minimizer $\boldsymbol{m}_2$ (activation path 17). The path leads to the third order saddle point $\boldsymbol{s}_{17}$. It passes through the symmetry-breaking double turning point $\boldsymbol{\vartheta}_5$ (= point 54 in table 4) at which two eigenvalues of the Hessian matrix become zero. Notice that the eigenvalue belonging to the antisymmetric eigenvector remains small along the remaining path segment. Beside the six zero eigenvalues the Hessian matrix $\boldsymbol{H}(\boldsymbol{s}_{17})$ possesses a very small eigenvalue ($|\lambda| = 0.001$ mdyn/Å). No decrease in the potential energy has been observed in the direction of the eigenvector.

A symmetric and a nonsymmetric relaxation path originate at the saddle point $\boldsymbol{s}_{17}$; see table 2. The symmetric relaxation path leads to the symmetric second order saddle point $\boldsymbol{s}_{15}$. Both transition vectors of the saddle point $\boldsymbol{s}_{15}$ are antisymmetric such that only nonsymmetric relaxation paths can originate at this saddle point. One nonsymmetric relaxation path ends at the first order saddle point $\boldsymbol{s}_{11}$ (path 20).

Also at the acetaldehyde minimizer $\boldsymbol{m}_1$ equilibrial path tracings have been started. The activation path determined by the normal mode vector $\boldsymbol{v}_2$ ends at the pitchfork bifurcation point $\boldsymbol{\psi}_6 = (\boldsymbol{b}_6, \rho_6)$. The kernel vector (listed in table 12) indicates a rotation of the CH_2 group about the CC axis such that the nonsymmetric paths will lead to the first order saddle points $\boldsymbol{s}_6$ and $\boldsymbol{S}\boldsymbol{s}_6$. The symmetric path originating at the bifurcation point ends at the second order saddle point $\boldsymbol{s}_7$ which determines the energy barrier between the saddle points $\boldsymbol{s}_6$ and $\boldsymbol{S}\boldsymbol{s}_6$. The energy difference between the saddle points $\boldsymbol{s}_6$ and $\boldsymbol{s}_7$ is small ($E(\boldsymbol{s}_6) - E(\boldsymbol{s}_7) = 0.15$ eV). In figure 8 the reaction topography is visualized. It results from the activation path 12 and the relaxation paths

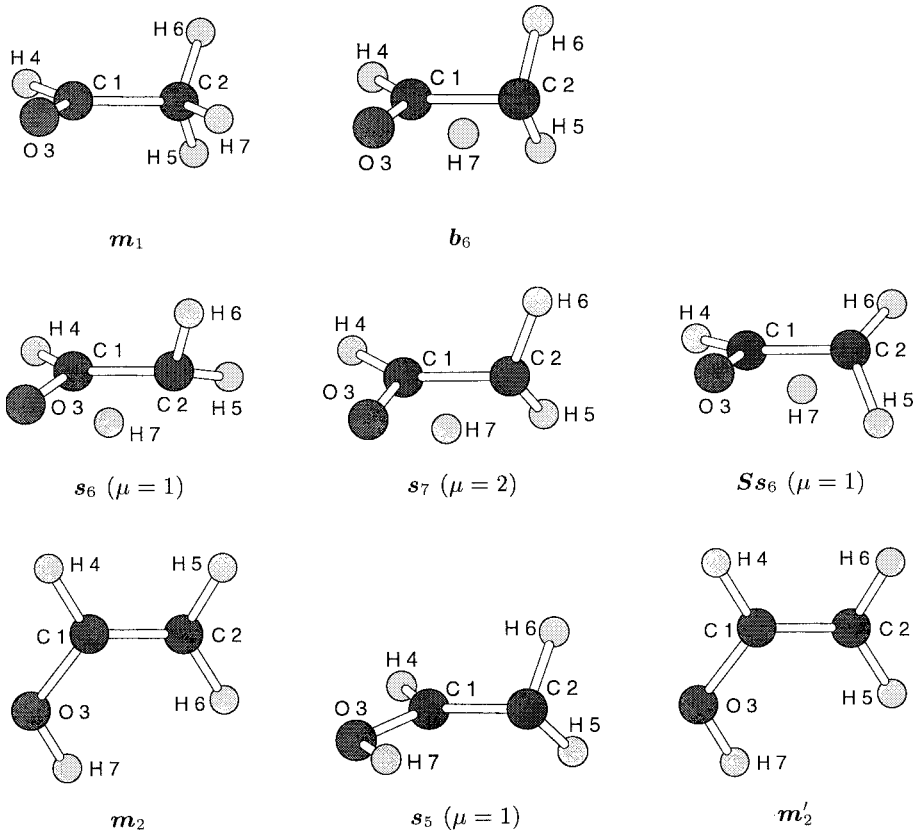

Figure 8. Isomerization acetaldehyde/vinyl alcohol.

24, 25 and 35. The transition structure s_5 is associated with a (perturbed) rotation of the CH_2 group about the CC axis in the vinyl alcohol molecule.

2.3. $C_2H_4O \rightarrow CH_4 + \overline{C}O$

The reaction topography of the elimination of methane from acetaldehyde is visualized in figure 9. It results from the activation path 8 and the relaxation paths 23 and 33. No bifurcation point has been detected along the activation path. It appears that the second order saddle point s_{10} which determines the energy barrier for the rotation of the CH_3 group about the CC axis takes the role of a symmetry-breaking bifurcation point. Notice that the difference in the potential energy of the first order saddle point s_9 and the second order saddle point s_{10} is very small (0.038 eV). The bifurcation point ϑ_7 appears to be a symmetry-breaking double turning point. It belongs to a segment of the relaxation path 33 where the Hessian matrix possesses three very small eigenvalues ($\leqslant 4 \cdot 10^{-3}$ mdyn/Å in magnitude). The point marks the change of the hydrogen nucleus H4 from the CO fragment to the CH_3 fragment. The minimizer m_0 appears to be

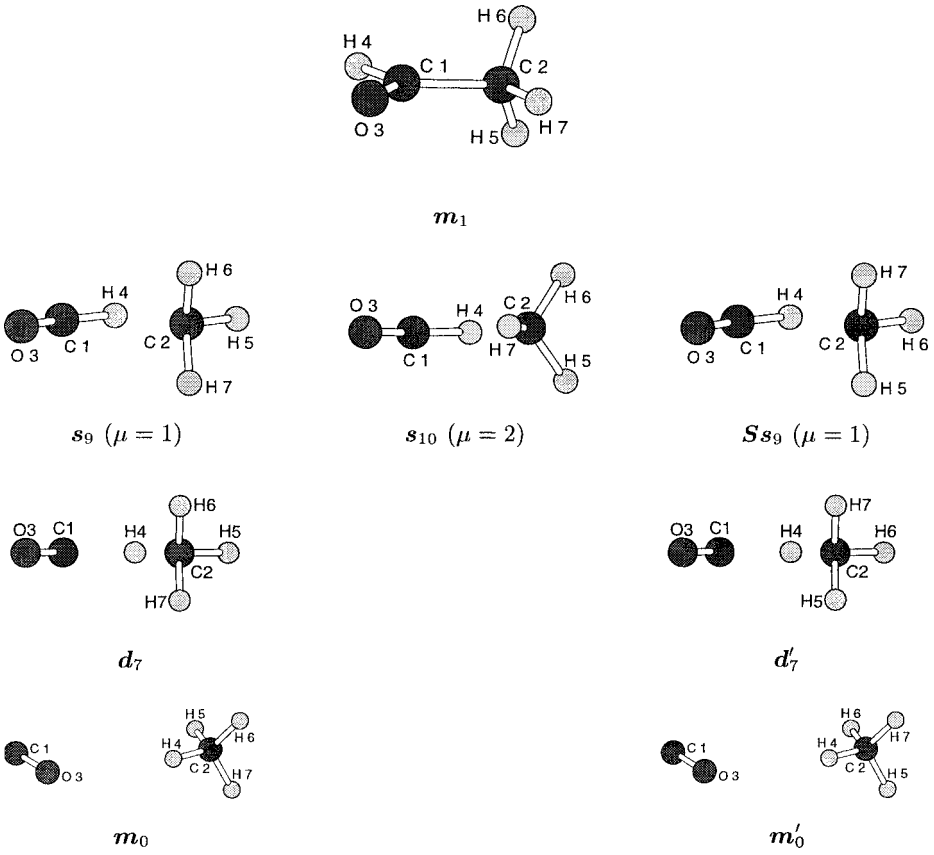

Figure 9. $C_2H_4O \rightarrow CH_4 + \overline{C}O$.

the global minimizer of the energy function. A minimizer that attains an energy value smaller than $E(\boldsymbol{m}_0)$ has not been found.

2.4. $C_2H_4O \rightarrow H_2O + \overline{C}_2H_2$

The elimination of water from vinyl alcohol is connected with the activation path 19 and the relaxation paths 16, 17 and 29. It is visualized in figure 10. The transition structure is defined by the saddle point $\boldsymbol{s}_{16}$. The saddle point $\boldsymbol{s}_{20}$ determines the energy barrier for the rotation of the nucleus H7 about the OH axis ($E(\boldsymbol{s}_{20}) - E(\boldsymbol{s}_{16}) = 0.56$ eV). The valley–ridge inflection configuration $\boldsymbol{b}_{12}$ has been found at the relaxation path 29 (table 11 shows the internal coordinates). The kernel vector indicates a rotation of the hydrogen nucleus H7 about the OH axis. Thus the branch bifurcating from relaxation path 29 should lead to the saddle point $\boldsymbol{s}_4$ which provides the rotational barrier of the water molecule in the water/vinylidene system ($E(\boldsymbol{m}_6) - E(\boldsymbol{s}_4) = 0.035$ eV). Along the primary path the H_2O fragment rotates through an angle of about 30 degrees about the CO axis. The Hessian matrix $\boldsymbol{H}(\boldsymbol{s}_4)$ possesses an eigenvector $\boldsymbol{e} \in (\mathbb{T} \oplus \mathbb{S}(\boldsymbol{s}_4))^{\perp}$ which

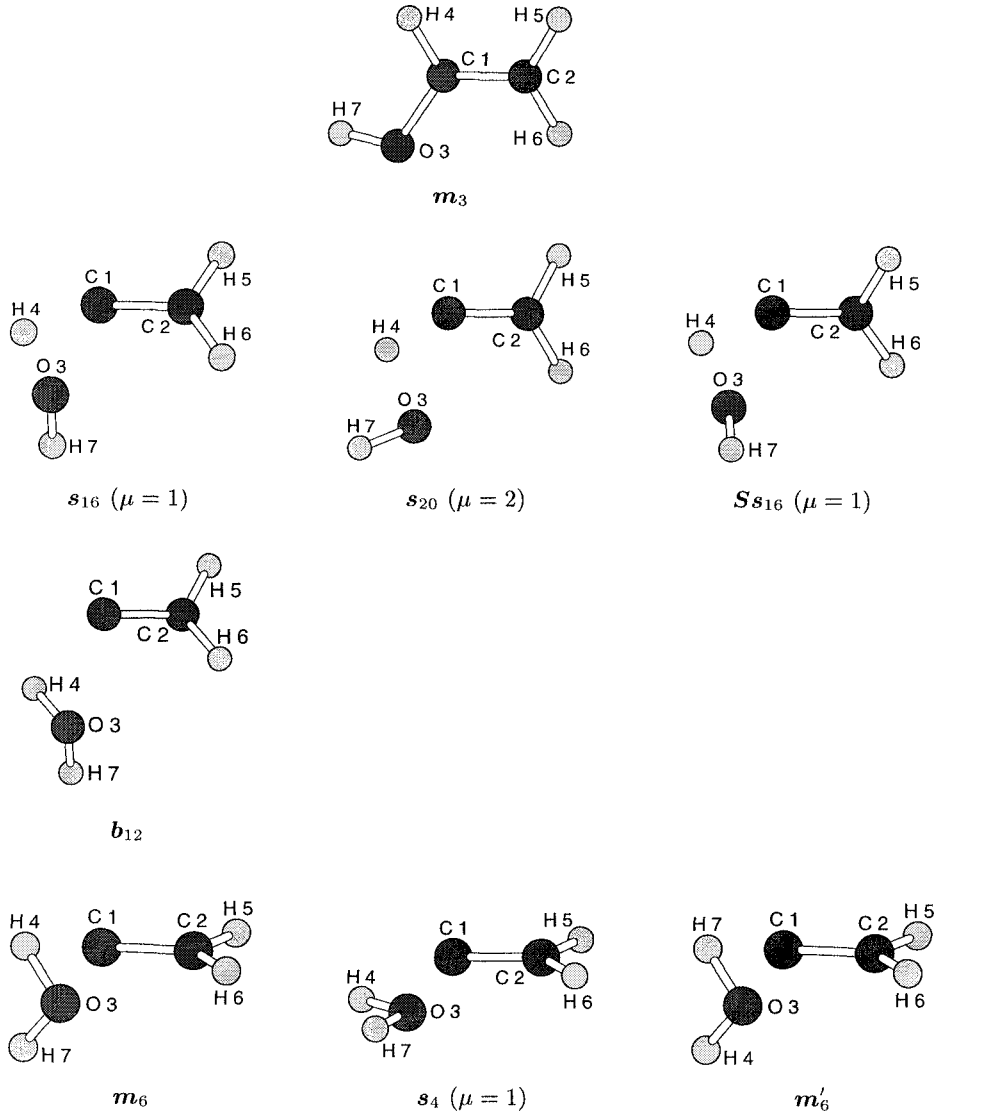

Figure 10. $C_2H_4O \rightarrow H_2O + \overline{C}_2H_2$.

belongs to an eigenvalue smaller than $< 4 \cdot 10^{-4}$ mdyn/Å in magnitude. This eigenvector indicates the separation of water and vinylidene. Thus in the vicinity of the saddle point s_4 the potential energy surface looks like a Lennard–Jones potential.

2.5. $C_2H_4O \rightarrow H_2CO + \overline{C}H_2$

The elimination of formaldehyde from acetaldehyde should be strict related to the reaction topography given in figure 11. The reaction topography has been gathered from the activation path 7 and the relaxation paths 5, 15, 19, 30 and 34. The differences

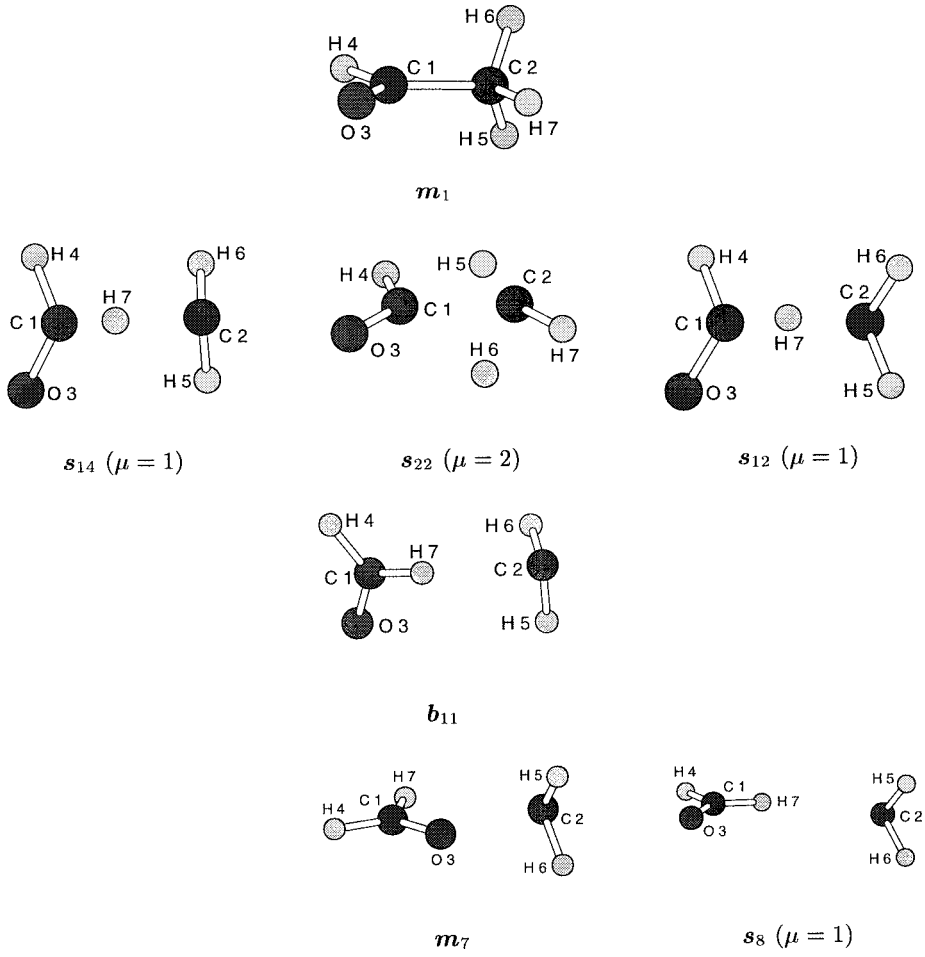

Figure 11. $C_2H_4O \rightarrow H_2CO + \overline{C}H_2$.

between the saddle points s_{23} and s_{22} should be negligible. Likely the saddle point s_{23} is an artifact. The valley–ridge inflection configuration b_{11} has been detected at the relaxation path 30. It connects the transition structures s_{12} and s_{14} by a rotation of the H_2CO fragment about the axis perpendicular to the plane spanned by both carbon nuclei and the hydrogen nucleus H7. Furthermore, it connects the transition structure s_{14} (respectively s_{12}) with the minimizer m_7 by a rotation of the H_2CO fragment about the CH axis. The energy and the internal coordinates of the configuration b_{11} are listed in table 11.

The saddle point s_8 determines the energy barrier that the system has to overcome before formaldehyde and methylene can separate.

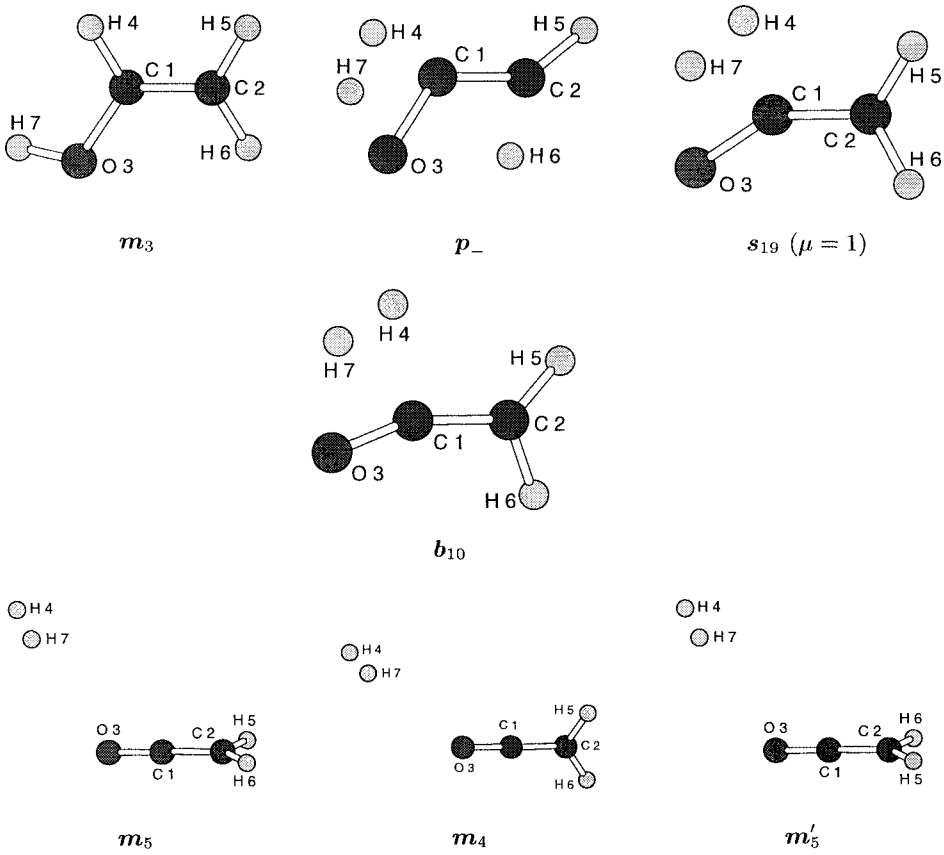

Figure 12. $C_2H_4O \rightarrow C_2H_2O + H_2$.

2.6. $C_2H_4O \rightarrow C_2H_2O + H_2$

This elimination is connected with the activation path 22 and the relaxation path 28. The characteristic configurations are depicted in figure 12.

In accordance with [1, theorem 8] the configurations remain planar along both paths. The activation path ends at the first order saddle point $\boldsymbol{s}_{19}$ which represents the transition structure. It passes through the turning point configuration $\boldsymbol{p}_-$ which is associated with the entry into the reactive domain. The relaxation path 28 ends at the minimizer $\boldsymbol{m}_4$. The behavior of the small eigenvalues along this path shows table 5. At point 22 which coincides with the bifurcation point $\boldsymbol{\psi}_{10} = (\boldsymbol{b}_{10}, \rho_{10})$ an eigenvalue of the Hessian matrix which belongs to an antisymmetric eigenvector changes its sign. Since the gradient vector $\mathbf{g}(\boldsymbol{b}_{10})$ is symmetric, $\boldsymbol{b}_{10}$ is a valley–ridge inflection point. Table 11 shows the internal coordinates of the configuration $\boldsymbol{b}_{10}$. Because λ_4 is the only non-trivial zero eigenvalue of the Hessian matrix $\boldsymbol{H}(\boldsymbol{b}_{10})$ (i.e., $\dim(\ker \boldsymbol{H}(\boldsymbol{b}_{10}) \cap \mathbb{P}_0) = 1$),

Table 6
Energies and internal coordinates of some stable configurations.

	m_0	m_4	m_5	m_6	m_7
E(m_i)	−152.9333	−152.8519	−152.8518	−152.7803	−152.7520
12		1.3053	1.3054	1.2942	
13	1.1140	1.1453	1.1452	2.8207	2.0683
14					1.0934
17					1.0934
23					1.1921
24	1.0835				
25	1.0837	1.0711	1.0711	1.0776	1.0837
26	1.0837	1.0711	1.0711	1.0761	1.0877
27	1.0838				
34	3.1756			0.9483	
37		3.0246	3.0998		
47		0.7301	0.7301		
125		119.33	119.32	119.72	
132					109.80
134	106.56				
137		122.86	137.64	79.40	
213		179.99	179.98	97.62	
314					90.00
325					121.17
374		172.13	169.97		
417					103.34
425	109.46				
426	109.46				
427	109.57				
437				104.86	
526	109.45	121.34	121.34	120.26	118.26
1325	116.32				0.00
1326	116.32				180.00
1327	0.00				
1342	0.00				
1374		0.00	0.00		
2134				126.26	
2137				−126.26	
2174		0.00	0.00		
2314					−128.33
2317					128.33
3125				180.00	
3126				0.00	
7325		89.99	0.00		
7326		−89.99	180.00		

the bifurcation point $\boldsymbol{\psi}_{10}$ is a symmetry-breaking pitchfork bifurcation point; see [1, theorem 10]. The symmetric branch arising at $\boldsymbol{\psi}_{10}$ passes through a turning point $\boldsymbol{p}_+$ which is lying between the points 29 and 30; see table 5. The turning point configuration has the appearance of the valley–ridge inflection configuration $\boldsymbol{b}_{10}$. The derivative $\dot{\rho}$ changes its sign after the eigenvalue has changed its sign. This delay is due to the fact that the eigenvalues have been calculated from exact Hessian matrices, but the path tracing procedure computes the tangents $\dot{\boldsymbol{z}} = (\dot{\boldsymbol{p}}, \dot{\rho})^\top$ from updated matrices; see [2]. In the vicinity of the minimizer $\boldsymbol{m}_4$ five eigenvalues approach zero (see table 5) since the symmetric branch leads into a *set* of minimizers (there is no uniquely determined minimizer). In figure 12 three snapshots ($\boldsymbol{m}_5$, $\boldsymbol{m}_4$ and $\boldsymbol{m}_5'$) are depicted. The minimizers $\boldsymbol{m}_4$ and $\boldsymbol{m}_5$ have been obtained by refining two (different) points of the final segment of the relaxation path 28. The configurations $\boldsymbol{m}_4$ and $\boldsymbol{m}_5$ possess two frequencies which are smaller than 34 cm^{-1} (in magnitude). One frequency is associated with the rotation of the ketene molecule about the CCO axis whereas the other is related to the separation of H_2 and OC_2H_2.

3. Note to tables 6–12

The internal coordinates of a configuration are described by means of the numbers of the nuclei. A pair ij denotes the distance between the ith and jth nucleus, a triplet ijk means the angle formed by the nuclei i, j, k, and $ijkl$ is the dihedral angle between the plane spanned by the nuclei i, j and k and the plane spanned the nuclei j, k, l. Distances are in Å, angles in degrees. The energy is in H.

4. Conclusions

The results reported in section 3 enable the following conclusions:

1. Potential energy surfaces possess many valley–ridge inflection points in general. Valley–ridge inflection points occur in particular when the C_s-symmetry of a molecular system is broken.

2. Frequently the transition structure of a reactive process has a lower symmetry than the educt and the product. Therefore many equilibrial paths pass through a symmetry-breaking bifurcation point. Regular equilibrial paths that join two stationary points are very rare.

3. Activation paths lead always to a saddle point (or fail). They do not lead necessarily to a saddle point of first order. Activation paths along which the symmetry is conserved end frequently at a saddle point of higher order. Nonsymmetric saddle points of first order may be obtained if at a symmetry-breaking pitchfork bifurcation point a nonsymmetric branch is followed.

Table 7
Internal coordinates of saddle point configurations s_i, $i = 1(1)10$.

	s_1	s_2	s_3	s_4	s_5	s_6	s_7	s_8	s_9	s_{10}
12	1.5101	1.3139	1.3179	1.2922	1.4244	1.4205	1.4609	3.8192	2.0677	2.1006
13	1.1878	1.3680	1.3201	3.4351	1.2730	1.2517	1.2423	1.1875	1.1458	1.1439
14	1.0944	1.0771	1.0764		1.0883	1.0807	1.0823	1.0931	1.0967	1.0938
17								1.0886		
25	1.0831	1.0739	1.0732	1.0768	1.0964	1.0785	1.0888	1.0955	1.0842	1.0870
26	1.0848	1.0750	1.0740	1.0779	1.0964	1.0847	1.0888	1.0955	1.0882	1.0870
27	1.0848								1.0842	1.0833
34				0.9486						
37		0.9478	0.9292	0.9473	0.9671	1.2343	1.1285			
125	111.95	120.42	119.39	121.33	105.74	120.72	110.91	122.02		
126	109.30	121.51	121.99	118.39	105.74	110.04	110.91			
137		110.24	180.00		104.29	79.79	85.69			
213	123.17	123.66	124.98	101.95	120.01	109.18	109.09	104.25	109.97	111.62
214	116.64	122.11	121.66	120.30	130.85	131.54	134.24			
314								121.49	163.39	164.41
317								122.29		
437				106.03						
526								103.53	110.28	110.16
527	109.27								110.28	110.32
627									110.78	110.32
2137		−85.70	180.00	180.00	0.00	−9.04	0.00			
3125	180.00	1.35	180.00	180.00	125.24	152.43	120.14	−67.88	180.00	115.07
3126	−58.79	−178.04	0.00	0.00	−125.24	−73.68	−120.14	67.88	−56.82	−115.07
3127	58.79							180.00	56.82	0.00
3147								180.00		0.00
4125	0.00	−0.71	0.00	180.00	−54.76	−24.80	−59.86		0.00	

Table 8
Internal coordinates of saddle point configurations s_i, $i = 10(1)20$.

	s_{11}	s_{12}	s_{13}	s_{14}	s_{15}	s_{16}	s_{17}	s_{18}	s_{19}	s_{20}
12	1.4434	2.1216	1.4623	2.1975	1.3835	1.2998	1.3708	1.3792	1.3138	1.2909
13	1.1908	1.1799	1.1953	1.1715	1.2207	1.7644	1.2326	1.2109	1.2611	1.8974
14	1.1079	1.0841	1.0913	1.0902	1.0909	1.2267	1.0872	1.0915	1.3356	1.1611
25	1.0846	1.0908	1.0826	1.0869	1.0654	1.0754	1.0659	2.1139	1.0699	1.0748
26	1.9474	1.0936	1.9333	1.0902	1.2517	1.0740	1.2412	2.1139	1.0743	1.0738
27	1.7723	1.6628	1.7282	1.3567	1.2967		1.3565	1.0597		
37						0.9527			1.3644	0.9533
125	113.42		113.91		140.33	117.93	142.54	100.97	121.88	118.18
126								100.97		
127								170.39		
137									58.91	
213	132.80	119.66	118.67	120.53	123.64	111.92	119.79	122.11	146.76	106.48
214	105.10		118.73		114.35	154.74	117.78	114.80	106.60	149.28
314		125.22		125.14						
437										90.92
526	86.61	106.64	83.96	107.86	96.73	119.02	100.50		120.40	120.34
527	97.28	89.48	97.05	100.40	133.39		137.37			
627		84.51		102.15						
2137						−82.34			180.00	180.00
3125	−105.29	−37.91	−69.83	18.86	180.00	−179.43	180.00	169.76	180.00	180.00
3126	−18.60	−150.42	−154.55	127.34	0.00	−0.20	0.00	−169.76	0.00	0.00
3127	−0.51		−174.48		0.00		0.00	0.00		
3147		167.44		167.46						
4125		179.20		−139.69	0.00	−178.78	0.00		0.00	180.00
4127	−0.51		12.58					180.00		

Table 9
Internal coordinates of saddle point configurations s_i, $i = 20(1)26$.

	s_{21}	s_{22}	s_{23}	s_{24}	s_{25}	s_{26}
12	2.3448	1.7071	1.6335	2.3738	2.0558	
13	1.1291	1.1613	1.1727	1.1247	1.1168	1.1793
14	1.2556	1.0770	1.0835	1.1315	1.0793	1.1099
25	1.0602	1.1299	1.1170	1.0956	1.1333	1.0801
26	1.0602	1.1299	1.1170	1.0956	1.1333	1.0801
27	1.0805	1.1051	1.1336	1.2871	1.0976	1.1236
37						1.9403
125		65.86	74.66		65.12	
142	96.71			99.86		
172						158.02
213	170.42	130.63	129.42		129.94	
314	138.41	128.57	124.88	157.30	157.16	120.85
317				121.17		87.46
526	128.17	108.64	114.50	104.86	105.03	112.90
627	115.48	86.60	73.81	100.09	97.92	119.75
2713				180.00		0.00
3125	91.91	62.89	60.70	64.74	61.01	98.61
3126	−91.91	−62.89	−60.70	−64.74	−61.01	−98.61
3127	0.00	0.00	0.00		0.00	
3142	180.00	180.00	180.00	180.00	180.00	
4137						180.00

4. Relaxation paths that originate at a saddle point of order μ, end in general at a stationary point of the order $\mu - 1$. Relaxation paths that start at a first order saddle point lead always to a minimizer (or fail). Generally relaxation paths that start at a symmetric saddle point of second order end at a nonsymmetric saddle point of first order if a nonsymmetric reaction vector is employed.

5. In the reactive processes two typical kinds of motions occur, namely translations and rotations of a group of nuclei. The group may consist of a single nucleus. Since a rotation may follow the positive or negative direction, the beginning of a rotation is always associated with a path branching. In other words, in a nuclear system the rotation of a group of nuclei sets in at a valley–ridge inflection point (simple bifurcation point), where some symmetry of symmetric configurations is broken.

6. The looseness necessary to rearrange the nuclei in a molecular system is made by adsorbing some energy *and* breaking some symmetry. Symmetry-breaking is preferred against the absorbation of additional energy.

Table 10
Energies and internal coordinates of some valley–ridge inflection configurations at activation paths.

	$\boldsymbol{b}_1$	$\boldsymbol{b}_2$	$\boldsymbol{b}_3$	$\boldsymbol{b}_4$	$\boldsymbol{b}_5$	$\boldsymbol{b}_6$	$\boldsymbol{b}_7$	$\boldsymbol{b}_8$	$\boldsymbol{b}_9$
E($\boldsymbol{b}_i$)	−152.911	−152.894	−152.868	−152.811	−152.774	−152.755	−152.738	−152.711	−152.692
12	1.512	1.519	1.328	1.316	1.469	1.420	2.324	1.541	1.823
13	1.191	1.198	1.358	1.310	1.166	1.229	1.156	1.244	1.167
14	1.079	1.120	1.090	1.062	1.131	1.072	1.130	1.057	1.126
25	1.096	1.085	1.088	1.146	1.104	1.098	1.049	1.171	1.109
26	1.096	1.085	1.097	1.160	1.100	1.098	1.049	1.171	1.109
27	1.059	1.063			1.126		1.150	1.166	1.089
37			0.924	0.946		1.225			
125	113.2	118.3	132.2	85.2	76.6	102.5	79.3	127.7	55.0
127	107.0	90.9			149.2		144.8	55.7	83.2
137			115.8	106.0		81.0			
213	128.5	112.3	109.4	139.8	137.1	111.3	117.4	114.1	126.3
214	109.0	127.7	135.4	103.4	86.9	121.2	135.7	126.5	
314									120.3
526	109.5	110.8	120.5	128.3	125.2	107.9	111.2	72.8	109.4
2137			−180.0	−180.0					
3125	117.4	111.2	−180.0	−180.0	114.6	124.1	123.0	131.4	93.6
3126	−117.4	−110.7	0.0	0.0	−113.8	−124.1	−122.8	−131.4	−92.8
3127	0.0	0.2			0.6	0.0	0.1	0.0	0.2
4126			180.0	180.0					
4127	−180.0	−179.8			−179.5	180.0	−179.9	180.0	179.8

Table 11
Energies and internal coordinates of some valley–ridge inflection configurations at relaxation paths.

	$\boldsymbol{b}_{10}$	$\boldsymbol{b}_{11}$	$\boldsymbol{b}_{12}$
E($\boldsymbol{m}_i$)	−152.728	−152.740	−152.771
12	1.309	3.018	1.294
13	1.191	1.187	2.287
14	1.606	1.091	
17	1.488	1.095	
25	1.075	1.094	1.075
26	1.074	1.096	1.066
34			0.952
37			0.940
125	131.4		115.0
134			50.5
172		119.3	
213	159.0		105.5
214	99.4		
314		122.1	
317	68.0	122.2	
417		115.7	
437			106.9
526	120.2	103.7	120.4
1725		−68.6	
1726		38.3	
2134	180.0		−175.2
2137	180.0		−79.1
2713		62.0	
2714		−117.7	
3125	180.0		178.4
3126	0.0		−2.7

7. Bifurcation points are of great importance for the understanding of reaction mechanisms. Therefore codes that refine guesses in an efficient manner are very necessary. Furthermore codes that compute the tangents to the bifurcating branches are needed.

5. Summary

The results of a comprehensive exploration of an *ab initio* potential energy surface of the C_2H_4O system are reported and discussed. The results indicate that equilibrial paths are a good means to locate both stationary points and valley–ridge inflection points, especially if only poor *a priori* information is available. Equilibrial paths enable to gain insight into the topography of a potential energy surface.

Table 12
Kernel vectors[1] of the simple bifurcation points $\boldsymbol{b}_i$, $i = 1(1)12$.

i	$\boldsymbol{b}_{i1}$	$\boldsymbol{b}_{i2}$	$\boldsymbol{b}_{i3}$	$\boldsymbol{b}_{i4}$	$\boldsymbol{b}_{i5}$	$\boldsymbol{b}_{i6}$	$\boldsymbol{b}_{i6}$
	0.000	0.000	0.000	0.000	0.231	0.232	0.000
1	0.000	0.000	0.000	0.000	0.358	−0.358	0.000
	0.050	−0.077	−0.189	0.459	−0.327	−0.327	0.410
	0.00	0.00	−0.01	0.00	−0.14	0.16	0.00
2	−0.01	0.01	−0.01	−0.02	0.36	−0.35	−0.02
	0.16	−0.15	0.53	0.06	−0.40	−0.40	0.06
	0.079	−0.201	0.324	0.348	−0.264	0.060	−0.347
3	−0.052	−0.182	−0.156	0.480	−0.376	0.315	−0.022
	0.000	0.000	0.000	0.000	0.000	0.000	0.000
	0.000	0.000	0.000	0.000	0.000	0.000	0.000
4	0.000	0.000	0.000	0.000	0.000	0.000	0.000
	0.132	−0.019	0.777	−0.371	0.142	−0.361	−0.300
	0.00	0.00	0.00	0.00	0.29	−0.29	0.00
5	0.00	0.00	0.00	0.00	0.05	−0.05	0.00
	−0.07	0.02	0.52	−0.64	−0.09	−0.09	0.36
	0.000	0.000	0.000	0.000	0.214	−0.214	0.000
6	0.000	0.000	0.000	0.000	0.501	−0.501	0.000
	0.104	0.324	−0.505	0.236	−0.089	−0.089	−0.016
	−0.152	0.251	−0.279	−0.541	0.209	0.209	0.303
7	−0.041	0.047	−0.520	0.243	0.122	0.122	0.027
	0.000	0.000	0.000	0.000	0.001	−0.001	0.000
	0.000	0.000	0.000	0.000	−0.180	0.180	0.000
8	0.000	0.000	0.000	0.000	0.050	−0.050	0.000
	−0.004	0.150	0.279	−0.868	0.197	0.197	0.049
	0.00	0.00	0.00	0.00	0.07	−0.07	0.00
9	0.00	0.00	0.00	0.00	−0.39	0.38	0.00
	0.37	−0.17	0.15	0.46	−0.17	−0.18	−0.47
	0.000	0.000	0.000	0.000	0.000	0.000	0.000
10	0.000	0.000	0.000	0.000	0.000	0.000	0.000
	0.173	−0.258	0.428	0.269	−0.110	−0.756	0.254
	−0.044	−0.019	0.208	−0.306	−0.046	0.241	−0.035
11	0.086	0.122	−0.001	0.182	−0.104	−0.362	0.078
	−0.039	0.134	−0.299	0.226	−0.453	0.478	−0.048
	−0.015	0.050	−0.011	−0.004	0.098	0.030	−0.149
12	0.035	−0.016	0.083	0.060	−0.020	−0.050	−0.092
	0.274	−0.256	0.352	0.231	−0.558	−0.416	0.378

[1]The eigenvalues are smaller than 6.7×10^{-4} in magnitude.

References

[1] W. Kliesch, Potential energy surface exploration with equilibrial paths. Part I: Theory, J. Math. Chem. 28 (2001) 91.
[2] W. Kliesch, *A Mechanical String Model of Adiabatic Chemical Reactions* (Springer, 1998).
[3] W. Kliesch, EQUIPATH – An equilibrial path tracing routine for use with the program package GAUSSIAN'94, Max Planck Institute for Mathematics in the Sciences, Leipzig (1998).
[4] M.J. Frisch, G.W. Trucks. H.B. Schlegel, P.M.W. Gill, B.G. Johnson, M.A. Robb, J.R. Cheeseman, T. Keith, G.A. Petersson, J.A. Montgomery, K. Raghavachari, M.A. Al-Laham, V.G. Zakrzewski, J.V. Ortiz, J.B. Foresman, J. Cioslowski, B.B. Stefanov, A. Nanayakkara, M. Challacombe, C.Y. Peng, P.Y. Ayala, W. Chen, M.W. Wong, J.L. Andres, E.S. Replogle, R. Gomperts, R.L. Martin, D.J. Fox, J.S. Binkley, D.J. Defrees, J. Baker, J.P. Stewart, M. Head-Gordon, C. Gonzalez and J.A. Pople, Gaussian 94, Revision E.1, Gaussian, Inc. (1995).
[5] C. Peng, P.Y. Ayala and H.B. Schlegel, J. Comp. Chem. 17 (1996) 49.
[6] Gauss View, Version 1.01, Gaussian, Inc. (1997).
[7] J. Andrés, L.R. Domingo, M.T. Picher and V.S. Safont, Intern. J. Quant. Chem. 66 (1998) 9.